UCLA
UCLA Previously Published Works

Title

Enhancing autophagy in CD11c+ antigen-presenting cells as a therapeutic strategy for acute respiratory distress syndrome

Permalink

https://escholarship.org/uc/item/4j3621xn

Journal

Cell Reports, 42(8)

ISSN

2639-1856

Authors

Quach, Christine

Helou, Doumet Georges

Li, Meng

et al.

Publication Date

2023-08-01

DOI

10.1016/j.celrep.2023.112990

Copyright Information

Peer reviewed

Enhancing autophagy in CD11c+ antigen-presenting cells as a therapeutic strategy for acute respiratory distress syndrome

Christine Quach[1], Doumet Georges Helou[1], Meng Li[2], Benjamin Pierre Hurrell[1], Emily Howard[1], Pedram Shafiei-Jahani[1], Pejman Soroosh[3], Jing-hsiung James Ou[1], Babak Razani[4,5], Virender Rehan[6], Omid Akbari[1,7,*]

[1]Department of Molecular Microbiology and Immunology, Keck School of Medicine, University of Southern California, Los Angeles, CA 90033, USA

[2]USC Libraries Bioinformatics Service, University of Southern California, Los Angeles, CA 90089, USA

[3]Janssen Research and Development, San Diego, CA 92121, USA

[4]University of Pittsburgh School of Medicine and UPMC, Pittsburgh, PA 15261, USA

[5]Pittsburgh VA Medical Center, Pittsburgh, PA 15240, USA

[6]Division of Neonatology, Lundquist Institute for Biomedical Innovation at Harbor-UCLA Medical Center, Torrance, CA 90502, USA

[7]Lead contact

SUMMARY

Acute lung injury (ALI) and acute respiratory distress syndrome (ARDS) are severe clinical disorders that mainly develop from viral respiratory infections, sepsis, and chest injury. Antigen-presenting cells play a pivotal role in propagating uncontrolled inflammation and injury through the excess secretion of pro-inflammatory cytokines and recruitment of immune cells. Autophagy, a homeostatic process that involves the degradation of cellular components, is involved in many processes including lung inflammation. Here, we use a polyinosinic-polycytidylic acid (poly(I:C))-induced lung injury mouse model to mimic viral-induced ALI/ARDS and show that disruption of autophagy in macrophages exacerbates lung inflammation and injury, whereas autophagy induction attenuates this process. Therefore, induction of autophagy in macrophages can be a promising therapeutic strategy in ALI/ARDS.

*Correspondence: akbari@usc.edu.

Graphical Abstract

In brief

Quach et al. demonstrate through several mouse models that autophagy deficiency in CD11c$^+$ APCs aggravates lung inflammation and injury in a poly(I:C) mouse model of viral-induced acute respiratory distress system (ARDS). Autophagy induction in CD11c$^+$ APCs is able to attenuate inflammation and injury.

INTRODUCTION

Acute lung injury (ALI) and acute respiratory distress syndrome (ARDS) are life-threatening clinical conditions that can develop as a consequence of diverse causes such as sepsis, mechanical lung injury, toxic inhalation, and viral respiratory infections, such as influenza A, herpes simplex virus (HSV), and severe acute respiratory syndrome coronavirus 2 (SARS-CoV-2). ALI/ARDS is prevalent in 10% of patients in the intensive care unit and has an overall mortality rate of 43%.[1] Clinically, ALI/ARDS is characterized by the acuity of onset, pulmonary edema, pulmonary infiltrates, and hypoxemia due to increased lung permeability caused by alveolar damage and loss of epithelial and endothelial integrity.[2,3] Current therapeutic options are limited, resulting in the frequent need for invasive procedures such as mechanical ventilation with high supplemental oxygen. Therefore, understanding the role of the immune system and identifying altered cellular processes implicated in viral-induced ALI/ARDS pathology can lead to novel therapeutic strategies.

According to the 2011 Workshop Report on ALI/ARDS by the American Thoracic Society, several animal models utilizing known initiating triggers of the disease have been developed to recapitulate the pathophysiology seen in human lungs.[4] For example, polyinosinic-polycytidylic acid (poly(I:C)), a synthetic analog of viral double-stranded RNA (dsRNA), can mimic the acute inflammation seen in viral-induced ALI/ARDS.[5–8]

Acute onset ALI/ARDS depends on innate immune cell activation involving resident alveolar macrophages, recruited inflammatory monocytes/macrophages, dendritic cells, and neutrophils. In particular, antigen-presenting cells (APCs), such as macrophages, play an integral role in disease pathogenesis by modulating the inflammatory response and participating in tissue repair.[9,10] Macrophages are highly plastic cells with versatile functional phenotypes depending on the microenvironment. Commonly, they come in two subsets: the classically activated pro-inflammatory macrophage (M1) or the alternatively activated anti-inflammatory macrophage (M2). In the early acute exudative phase of ALI/ARDS, pulmonary macrophages are polarized to an M1 phenotype, resulting in the secretion of pro-inflammatory cytokines such as CXCL10, CXCL1, CCL2, interleukin-6 (IL-6), and tumor necrosis factor α (TNF-α) that can evoke severe lung inflammation and injury.[9] Additionally, these chemokines recruit other immune cells such as neutrophils and inflammatory monocytes/macrophages to further perpetuate lung inflammation and injury. In the reparative fibroproliferative phase of ALI/ARDS, M2-polarized macrophages contribute to tissue repair.[9]

Autophagy is an evolutionarily conserved process that is responsible for the regulated degradation and recycling of intracellular components to maintain homeostasis.[11] The process involves the formation of a double-membrane vesicle, the autophagosome, around the cytoplasmic components targeted for degradation.[11–13] Fusion of the autophagosome with the lysosome leads to enzymatic hydrolysis of the cytoplasmic cargo and release of metabolites that can be reused by the cell.[13] Autophagy was originally found to be a starvation response but now has been implicated in many health processes across various organs.[13] It plays an important role in both innate and adaptive immune response by targeting pathogens for degradation, producing peptides for antigen presentation, regulating inflammation, and controlling cell survival.[14,15] Given that autophagy dysfunction has been shown to promote neurodegeneration, hepatic dysfunction and tumor formation and to increase inflammation, it may be a promising therapeutic target in alleviating many diseases.[13,16–18] Autophagy is especially important for regulating phagocytosis, antigen presentation, and M1/M2 polarization in macrophages.[19,20] Our group previously demonstrated that deletion of autophagy-related gene 5 (*Atg5*), an essential autophagy protein, specifically in CD11c$^+$ APCs resulted in increased lung inflammation, neutrophilia, and increased airway hyperreactivity (AHR) in a mouse model of asthma.[21] However, the role of autophagy in CD11c$^+$ cells in the development of viral-induced ALI/ARDS remains unknown.

In the current study, we utilized a poly(I:C) mouse model to simulate viral-induced ARDS. Additionally, we developed mice with a deletion of *Atg5* specifically in CD11c$^+$ APCs to impair autophagy and mice with overexpression of transcription factor EB (*Tfeb*), a master inducer of autophagy, in CD11c$^+$ APCs to constitutively stimulate the autophagic

response.[22,23] Using these mice models of autophagy modulation, we observed reciprocal responses where a lack of autophagy led to increased lung inflammation and injury, while autophagy induction attenuated these deleterious outcomes. Furthermore, we examined the therapeutic effect of an autophagy inducer, α4-viral Fas-associated death domain-like IL-1β-converting enzyme-inhibitory protein (α4-vFLIP), in our poly(I:C)-induced lung injury mouse model.[24] This peptide had been demonstrated to robustly induce autophagy.[24] Administration of α4-vFLIP to poly(I:C)-stimulated mice effectively ameliorated secretion of pro-inflammatory cytokines and immune cell infiltration into the lung and reduced leakage of protein into the lung. Overall, our data support the activation of autophagic pathways in macrophages as a promising target for ALI/ARDS therapeutics.

RESULTS

Poly(I:C) stimulation induces lung inflammation and injury

To study viral-induced ALI/ARDS pathology, we needed to establish a mice model that could recapitulate the acute lung inflammation and injury seen in patients with ALI/ARDS. Therefore, we utilized poly(I:C), a synthetic viral dsRNA analog capable of initiating acute lung inflammation and injury. Mice were intranasally (i.n.) administered poly(I:C) (40 μg in 40 μL) or PBS over 3 consecutive days (Figure 1A). On day 4, lung function was evaluated by direct measurement of lung resistance and dynamic compliance in anesthetized and tracheostomized mice followed by analysis of the bronchoalveolar lavage fluid (BALF) and lungs. Basal lung resistance was not significantly different between poly(I:C)-treated mice and PBS-treated mice. Intriguingly, i.n. administration of poly(I:C) demonstrated significantly increased lung resistance upon increasing doses of methacholine challenge compared with mice administered PBS (Figure 1B). Poly(I:C)-treated mice also showed significantly lower dynamic compliance (Figure 1C). Taken together, the results indicate that poly(I:C) treatment compromised lung function.

Histological examination revealed an influx of immune cells into the lung tissue of poly(I:C)-treated mice, increased airway wall thickness, and a narrowing of the airways compared with PBS-treated mice (Figures 1D and 1E). Poly(I:C)-treated mice had concomitant massive infiltration of $CD45^+$, $CD11c^+$ APCs, $Gr1^+$ cells, and lymphocytes ($CD3^+$ and $CD19^+$ cells) in the BALF and lung (Figures 1F, 1G, and S1A). The increase in $Gr1^+$ cells were shown to be $CD11c^-Gr1^+Ly6C^{int}$ neutrophils and $CD11c^-Gr1^+Ly6C^{hi}$ monocytes (Figure S1B). Lastly, poly(I:C) stimulation induced significant recruitment of $CD45^+CD11c^+$ $CD11b^+CD64^+$ macrophages (Figures S1B and S1C). Additionally, we observed high levels of pro-inflammatory cytokines CXCL10, CXCL1, CCL2, CCL5, IL-1β, IL-6, and TNF-α in the BALF of poly(I:C)-treated mice compared with PBS-treated mice (Figure 1H).

We next assessed lung injury by comparing lung permeability between poly(I:C)-treated mice and PBS-treated mice. We performed fluorescein isothiocyanate (FITC)-labeled dextran assay by instilling mice i.n. with FITC-dextran and measuring fluorescence in the plasma. Poly(I:C) treatment induced significant leakage of FITC-dextran from the alveolar space to the blood compared with PBS-treated mice (Figure 1I). Poly(I:C) also induced increased protein concentration in the BALF (Figure 1J). These results provide

a characterization of lung function and immune response in a Poly(I:C) mouse model of viral-induced ALI/ARDS.

Poly(I:C) stimulation downregulates autophagy in CD11c+ APCs

APCs are the major orchestrators of lung inflammation and injury in ALI/ARDS.[9,10] In the lung, macrophages and dendritic cells express CD11c+.[10] Because we previously observed that a disruption of autophagy in murine CD11c+ APCs resulted in unprovoked lung inflammation, we wondered whether autophagy in CD11c+ APCs also played a role in the lung inflammation of ALI/ARDS.[21] First, we evaluated the specific composition of the CD11c+ APCs and observed that upon poly(I:C) administration, this population was predominantly macrophages, and the remaining population was predominantly dendritic cells (DCs) and Ly6C+ cells (Figures S1B and S1C). Additionally, poly(I:C) administration resulted in an increase in the frequency of CD11c+CD11b+CD64+ recruited macrophages, whereas PBS control mice had a larger frequency of CD11c+CD11b−CD64+ alveolar macrophages (Figures S1B and S1C). There were no significant differences in the frequency of DCs and Ly6C+ cells from CD45+CD11c+ cells regardless of genotype and treatment (Figure S1C). Autophagy is known to play a role in antigen presentation and the control of inflammasome activity in APCs, whereas viruses can either inhibit or induce autophagy to gain an advantage over the host.[12,15] Therefore, to explore the impact of poly(I:C) treatment on autophagy *in vivo*, we treated mice with poly(I:C) or with PBS (Figure 1A) and isolated CD11c+ and CD11c− cells from lung tissue. Sorted cells were lysed and immunoblotted for the autophagosome marker LC3 and for p62, an autophagy chaperone that serves as a link between LC3 and ubiquitinated cytoplasmic cargo to be degraded.[13,25] Because autophagy is a dynamic process, the gold standard for measuring autophagic flux is by measuring LC3 processing and p62 degradation by western blot.[25,26] Upon autophagy induction, LC3-I in the cytosol is lipidated to LC3-II, which becomes a part of the autophagosome membrane. At the end of the autophagic flux, p62 inside the autophagosome is degraded along with the cytosolic components.[13] Interestingly, we observed that CD11c+ cells from poly(I:C)-treated mice expressed less LC3-I and LC3-II and had significant accumulation of p62 compared with CD11c+ cells from PBS control mice, indicating a block in autophagic flux (Figures 2A–2C). On the other hand, PBS-treated CD11c− cells had a higher LC3-II/LC3-I ratio compared with their respective CD11c+ cells (lane 1 vs. lane 3) (Figures 2A–2C). Poly(I:C)-treated CD11c− cells had comparable LC3-II/LC3-I ratios (lane 2 vs. lane 4) to CD11c+ cells and lower levels of p62, indicating progression of autophagic flux. Interestingly, PBS- and poly(I:C)-treated CD11c− cells had lower band intensity for LC3 and p62 compared with their respective CD11c+ cell counterparts, suggesting generally that autophagy may be more active overall in CD11c+ cells. To further confirm autophagy status, we used THP-1-DifluohLC3 cells, which are THP-1 cells with tandem-tagged GFP-RFP-LC3, to measure autophagic flux. The GFP is acid sensitive and therefore degrades upon autophagosome fusion with lysosome, whereas the RFP is acid stable and will not degrade.[27] Therefore, measuring the GFP/RFP ratio in flow cytometry is indicative for autophagic flux activity. We confirmed that poly(I:C) treatment resulted in a high GFP/RFP ratio, indicating low autophagic flux (Figure S2A).[27] To further confirm our results, we performed confocal microscopy to visually observe fluorescent puncta formation. GFP+RFP+ (yellow) puncta represent autophagosomes, whereas RFP+ puncta represent autophagosomes that have fused

with lysosomes to degrade the GFP signal. Therefore, autophagic flux can be measured by the number of GFP$^+$RFP$^+$ (yellow) puncta and RFP$^+$ puncta. Representative confocal images showed a lack of RFP$^+$ puncta and accumulation of GFP$^+$RFP$^+$ (yellow) puncta in poly(I:C)-treated cells, whereas PBS-treated cells had a higher number of RFP$^+$ puncta (Figure S2B). Altogether, our results strongly suggests that poly(I:C) stimulation blocks autophagy in APCs.

Lack of autophagy in pulmonary CD11c$^+$ APCs exacerbates lung inflammation and injury

We used our Atg5^{KO} (knockout) mice to further confirm that autophagy in pulmonary CD11c$^+$ APCs played a role in propagating lung hyperinflammation and injury. Atg5^{KO} and Atg5$^{flox/flox}$ control mice were treated i.n. with poly(I:C) or PBS according to the same schedule as shown in Figure 1A. We observed that poly(I:C)-treated Atg5^{KO} mice had increased lung resistance and decreased dynamic compliance compared with poly(I:C)-treated Atg5$^{flox/flox}$ mice (Figures 3A and 3B). Histological examination of lung tissue revealed significant influx of immune cells and increased airway thickness in the lung tissue of poly(I:C)-treated Atg5^{KO} mice compared with poly(I:C)-treated Atg5$^{flox/flox}$ control mice (Figures 3C and 3D). Poly(I:C) treatment increased the number of CD45$^+$ cells, Gr1$^+$ cells, and lymphocytes in the BALF and lungs of mice regardless of genotype compared with PBS treatment (Figures 3E and 3F). Additionally, poly(I:C)-treated Atg5^{KO} mice had a significantly higher total number of Gr1$^+$ cells and lymphocytes in lung compared with poly(I:C)-treated control mice (Figures 3E and 3F). However, there were no significant differences in the number of CD11c$^+$ APCs in the BALF and lungs regardless of genotype and treatment (Figures 3E and 3F). Of note, total CD45$^+$ cells in poly(I:C)-treated Atg5^{KO} mice increased compared with poly(I:C)-treated control mice in the lungs and BALF, even though the increase was not statistically significant (Figures 3E and 3F). Poly(I:C) administration induced significant recruitment of CD45$^+$CD11c$^+$CD11b$^+$CD64$^+$ macrophages in the lungs compared with PBS treatment, which had a larger frequency of CD45$^+$CD11c$^+$CD11b$^-$CD64$^+$ alveolar macrophages (Figures S3A–S3C). However, there was no significant difference in the frequency of CD45$^+$CD11c$^+$CD11b$^+$CD64$^+$ macrophages between poly(I:C)-treated Atg5$^{flox/flox}$ and Atg5^{KO} mice (Figures S3A–S3C). We also observed significantly higher levels of pro-inflammatory cytokines CXCL10, CXCL1, CCL2, CCL5, IL-1β, IL-6, and TNF-α in the BALF of poly(I:C)-treated Atg5^{KO} mice compared with poly(I:C)-treated Atg5$^{flox/flox}$ mice (Figure 3G). Lastly, poly(I:C) treatment induced significant leakage of FITC-dextran from the alveolar space to the blood and increased protein concentration in the BALF of Atg5^{KO} compared with Atg5$^{flox/flox}$ control mice (Figures 3H and 3I). Altogether, these results demonstrate that autophagy deficiency results in lung hyperinflammation and injury upon poly(I:C) treatment.

Autophagy induction in pulmonary CD11c$^+$ APCs attenuates lung inflammation and prevents lung injury

To explore if autophagy induction in pulmonary CD11c$^+$ APCs could attenuate lung inflammation and injury, we evaluated the response of mice with an overexpression of Tfeb specifically in CD11c$^+$ cells (Tfeb^{TG}) to observe the effect of poly(I:C) treatment. Tfeb^{TG} and Tfeb$^{flox/flox}$ control mice were treated i.n. with poly(I:C) or with PBS (Figure 1A). We observed that poly(I:C)-treated Tfeb^{TG} mice had decreased lung resistance and increased

dynamic compliance compared with poly(I:C)-treated control mice (Figures 4A and 4B). Histological examination revealed little influx of immune cells and decreased airway thickness in the lung tissue of poly(I:C)-treated Tfeb[TG] mice compared with poly(I:C) treated control mice (Figures 4C and 4D). Poly(I:C)-treated Tfeb[TG] mice had no significant changes in the numbers of CD45^{+}, CD11c^{+} APCs, Gr1^{+} cells, and lymphocytes in the lung compared with poly(I:C)-treated control mice (Figure 4E). However, there were significantly decreased numbers of CD45^{+} and Gr1^{+} cells in the BALF of poly(I:C)-treated Tfeb[TG] mice compared with poly(I:C)-treated control mice (Figure 4F). There were no significant differences in total immune cell number between PBS-treated Tfeb[TG] mice and control mice (Figures 4E and 4F). While poly(I:C) administration induced significant recruitment of CD45^{+}CD11c^{+}CD11b^{+}CD64^{+} macrophages compared with PBS administration, there was no significant difference in the frequency between poly(I:C)-treated Tfeb[flox/flox] and Tfeb[TG] mice (Figures S4A–S4C). The majority of macrophages in PBS control mice were composed of CD45^{+}CD11c^{+}CD11b^{−}CD64^{+} alveolar macrophages (Figure S4C). Lastly, the frequency of DCs and Ly6C^{+} cells from CD45^{+}CD11c^{+} APCs remained unchanged regardless of genotype or treatment (Figure S4C). We also observed significantly lower levels of pro-inflammatory cytokines CXCL10, CXCL1, CCL5, IL-6, and TNF-α and no changes in CCL2 and IL-1β in the BALF of poly(I:C)-treated Tfeb[TG] mice compared with poly(I:C)-treated control mice (Figure 4G). Lastly, there were no differences in FITC-dextran leakage and total protein concentration in the BALF between poly(I:C)-treated Tfeb[TG] mice and poly(I:C)-treated control mice (Figures 4H and 4I). Altogether, these results suggest that autophagy induction can alleviate lung hyperinflammation and injury upon poly(I:C) treatment.

A lack of autophagy significantly impacts gene expression of pro-inflammatory cytokines

M1 and M2 macrophages have different transcriptional programs that dictate their functional phenotypes. Since macrophages constitute the majority of our CD11c^{+} APCs, we used RNA sequencing to evaluate the impact of autophagy on the transcriptome. We bred mice with a knockout of *Atg5* (Atg5[KO]) or overexpression of *Tfeb* (Tfeb[TG]) only in CD11c^{+} cells to study the effect of autophagy after poly(I:C) stimulation. *Atg5* is a required autophagy protein involved in the elongation and progression of autophagosome formation, whereas *Tfeb* is a master regulator of autophagylysosome biogenesis and an inducer of autophagy.[22,28,29] We found that a lack of autophagy significantly impacts gene expression compared with autophagy induction (Figures 5A and 5B). Interestingly, genes that were significantly upregulated in Atg5[KO] mice were significantly downregulated in Tfeb[TG] mice. For example, pro-inflammatory cytokines such as CXCL10, CCL2, CCL5, TNF-α, and IL-6 were significantly upregulated in Atg5[KO] mice, whereas these same cytokines were downregulated in Tfeb[TG] mice compared with their respective control mice (Figures 5C and 5D). Macrophages in Atg5[KO] mice were polarized toward an M1 phenotype, as they highly expressed Nos2, CXCL10, IL6, Stat1, and CCL2 compared with Tfeb[TG] mice, which had significantly decreased expression of M1 markers and increased expression for M2-related markers (Figures 5E and 5F). Atg5[KO] mice had significantly more total M1 macrophages in the lungs compared with Atg5[flox/flox] mice upon poly(I:C) administration; however, there were no significant differences in the number of M2 macrophages between Atg5[KO] and Atg5[flox/flox] mice (Figures 5G and

S5A). In support of this, the frequency of $CD45^+CD11c^+CD11b^+CD64^+$ macrophages expressing CD86, a marker associated with M1 macrophages, was significantly increased in Atg5[KO] mice compared with Atg5[flox/flox] control mice (Figure 5H). In contrast, the frequency of $CD45^+CD11c^+$ $CD11b^+CD64^+$ macrophages expressing CD206, CD163, and CD36, markers associated with M2 polarization, was significantly decreased in Atg5[KO] mice (Figures 5I–5K). These results show that a lack of autophagy highly affects the transcriptomic profile of $CD11c^+$ cells compared with autophagy induction, suggesting that autophagy deficiency promotes an activated and pro-inflammatory phenotype after poly(I:C) stimulation.

Use of an autophagy inducer, α4-vFLIP, ameliorates lung inflammation and injury

Our collaborator, Dr. Jae Jung, originally described a peptide called α4-vFLIP.[24] The peptide was derived from viral-encoded FLICE inhibitory protein (viral FLIP) encoded by Kaposi's sarcoma-associated virus and conjugated to *trans*-activator of transcription (TAT) for cell entry.[24] A predominant effect of α4-vFLIP involves induction of autophagy both *in vitro* and *in vivo*.[24,30] We confirmed that α4-vFLIP significantly induced autophagy in $CD11c^+$ APCs and in THP-1-DifluohLC3 cells (Figures 6A, 6B, and S6A–S6C). Given our promising results demonstrating autophagy induction in the attenuation of lung inflammation, we used α4-vFLIP to further confirm that targeting autophagy in pulmonary $CD11c^+$ APCs could be a viable treatment in reducing or preventing lung hyperinflammation and injury in ALI/ARDS.[24] C57BL/6 mice were treated i.n. with poly(I:C) or PBS and 8 h later were treated with α4-vFLIP or TAT, the control peptide, for 3 consecutive days (Figure 6A). On day 4, we measured lung function followed by lung and BALF analysis. We observed that α4-vFLIP-treated mice had decreased lung resistance and increased dynamic compliance compared with mice treated with either poly(I:C) alone or both poly(I:C) and TAT (Figures 6C and 6D). Histological examination revealed no influx of immune cells and decreased airway thickness in the lung tissue of α4-vFLIP-treated mice compared with poly(I:C) alone or both poly(I:C) and TAT (Figures 6E and 6F). There were also no significant differences compared to PBS control mice. Furthermore, the α4-vFLIP-treated mice had a significantly lower total number of $CD45^+$, $Gr1^+$ cells, and lymphocytes in the BALF and lung compared with poly(I:C) alone or both poly(I:C) and TAT (Figures 6G and 6H). Significantly lower levels of pro-inflammatory cytokines CXCL10, CXCL1, CCL2, CCL5, IL-1β, IL-6, and TNF-α were also observed in the BALF of α4-vFLIP-treated mice (Figure 6I).

Lastly, α4-vFLIP was able to decrease lung permeability as indicated by the significant decrease in FITC-dextran leakage and total protein concentration in the BALF (Figures 6J and 6K). Altogether, these results further support the benefits of autophagy induction in $CD11c^+$ APCs to alleviate lung hyperinflammation and injury instigated by poly(I:C) treatment.

DISCUSSION

In the present study, we aimed to illuminate a mechanism that could be targeted for pharmacological therapy to increase the repertoire of treatment options for ALI/ARDS. We

observed that poly(I:C) stimulation downregulated autophagy in CD11c$^+$ cells, which played a significant role in propagating lung hyperinflammation and injury in a mouse model of viral-induced ALI/ARDS. Administration of poly(I:C), a dsRNA analog, has been shown to fulfill the requirements set by the 2011 American Thoracic Society Workshop on defining the cardinal features of rapid-onset ALI/ARDS in experimental animal models.[4–6,31] These include histological evidence of tissue injury, alteration of the alveolar-capillary barrier, an inflammatory response, and evidence of physiological dysfunction.[4] Therefore, we adapted this model to study ALI/ARDS and successfully demonstrated that poly(I:C) stimulation resulted in mice with compromised lung function, increased lung inflammation, and increased lung permeability. On the other hand, lipopolysaccharide (LPS), a component of the bacterial cell wall, has also been used to induce ALI.[32,33] However, the LPS model stimulates Toll-like receptor 4 (TLR4) signaling, modeling a bacterial infection, whereas poly(I:C), like viral RNA, stimulates TLR3 signaling to model a respiratory viral infection, which makes it especially relevant given the recent SARS-CoV-2 pandemic and the seasonal occurrence of influenza.

The pathophysiology of ALI/ARDS is orchestrated by innate immune cells, particularly APCs that provide the first line of defense in the lung. These APCs are the major source of pro-inflammatory cytokines found in the BALF of patients with ALI/ARDS.[34,35] In our poly(I:C) model, the CD11c$^+$ APCs in the BALF and lung were predominantly composed of macrophages, and poly(I:C) administration resulted in an influx of recruited CD45$^+$CD11c$^+$CD11b$^+$CD64$^+$ macrophages with concomitant loss of the CD45$^+$CD11c$^+$CD11b$^-$CD64$^+$ alveolar macrophage population compared with PBS administration. Since macrophages are highly plastic cells with functions dictated by the microenvironment, the polarization to classically activated M1 or alternatively activated M2 can govern the outcome in lung inflammation and injury. Prolonged M1 polarization leads to an excessive inflammatory response. Our transcriptomic data confirmed that CD11c$^+$ APCs from poly(I:C)-stimulated Atg5^{KO} mice highly upregulated M1 macrophage markers, whereas CD11c$^+$ APCs from Tfeb^{TG} mice upregulated M2 markers and significantly downregulated M1 markers, indicating that autophagy deficiency supports an inflammatory environment. Unsurprisingly, this led to increased pro-inflammatory cytokine secretion that was able to induce significant recruitment of neutrophils and monocytes/macrophages. Liu et al. found that impaired autophagy was associated with altered macrophage polarization skewing more toward an M1 phenotype.[36] Depletion of pulmonary macrophages has been shown to mitigate lung injury by attenuating neutrophil and monocyte recruitment and reducing pro-inflammatory cytokine secretion, highlighting the importance of macrophage activity in ALI/ARDS pathology.[37]

Our results demonstrated that CD11c$^-$Gr1$^+$ cells were significantly increased upon poly(I:C) stimulation compared with PBS treatment across all mice groups. These CD11c$^-$ Gr1$^+$ cells represented an influx of CD11c$^-$ Gr1$^+$ Ly6C^{int} neutrophils and CD11c$^-$ Gr1$^+$ Ly6C^{hi} monocytes to the lungs.[38,39] Autophagy deficiency in poly(I:C)-treated mice resulted in significantly increased numbers of CD11c$^-$Gr1$^+$ cells, whereas autophagy induction in poly(I:C)-treated mice resulted in attenuated numbers in the lungs and BALF. We observed that poly(I:C)-treated Atg5^{KO} mice showed no significant differences in total CD11c$^+$ cell numbers compared with Atg5$^{fl/fl}$ mice. Both poly(I:C)-treated Atg5^{KO} and Atg5$^{fl/fl}$ mice had

an increase in the frequency of recruited macrophages, but it was not significantly different. This suggests that autophagy deficiency in CD11c^{+} cells, which are composed primarily of macrophages, may likely affect their cytokine production capacity to increase recruitment of neutrophils and monocytes into the lungs.[1,15,37]

Our lab previously observed that a lack of autophagy in CD11c^{+} cells led to spontaneous unprovoked lung inflammation and neutrophilia in mice and liver inflammation in a mouse model of non-alcoholic fatty liver disease (NAFLD).[17,21] This suggests a role of autophagy in CD11c^{+} cells in propagating inflammation; therefore, we decided to observe the role of autophagy in CD11c^{+} cells in ALI/ARDS. We demonstrated that autophagy specifically in CD11c^{+} cells was highly affected by poly(I:C) stimulation, leading to increased inflammation. Disturbances to autophagy are implicated in numerous disease processes such as cancer, neurodegenerative diseases, metabolic disorders, and immune diseases.[12,40] In macrophages, defects in autophagy result in an inability to recycle damaged organelles, leading to the production of reactive oxygen species (ROS) and the leakage of mitochondrial DNA into the cytosol, which ultimately affects cell survival and clearance of dying cells.[11] Additionally, autophagy is key in regulating M1/M2 macrophage polarization in order to modulate the inflammatory response.[20] Several studies support the induction of autophagy in polarizing macrophages toward an anti-inflammatory phenotype to dampen the inflammatory response.[41–43] In DCs, autophagy participates in antigen presentation.[11,15] Autophagy inhibits the secretion of IL-1β and IL-18 in macrophages by regulating inflammasome activity, which has been shown to protect against ARDS induced by mechanical ventilation and LPS.[44] Interestingly, we observed that upon poly(I:C) induction, CD11c^{+} cells displayed impaired autophagy.

In our mice models, autophagy deficiency led to increased lung inflammation as demonstrated by immune cell infiltration and secretion of pro-inflammatory cytokines and chemokines, especially *Cxcl10* and *Ccl2*. Patients with ALI/ARDS show unusually high expression of CXCL10 and CCL2.[45,46] Indeed, others have explored the possibility of neutralizing these chemokines in regulating inflammation. For example, one study found that CXCL10 neutralization was found to ameliorate LPS-induced ALI/ARDS in rats.[47] Another study showed that CCL2 neutralization can reduce neutrophil recruitment, which in turn can prevent lung injury.[46] Therefore, targeting autophagy may control CXCL10 and CCL2 secretion, thus controlling neutrophil and monocyte recruitment.[39] Remarkably, autophagy induction showed completely opposite effects to autophagy deficiency. This was clearly seen in our RNA sequencing (RNA-seq) analysis demonstrating that the cytokines that were highly upregulated in Atg5[KO] mice were highly downregulated in Tfeb[TG]. Our autophagy-efficient Tfeb[TG] mice demonstrated reduced pro-inflammatory cytokines in the BALF, including CXCL10 and CCL2.

We showed that treatment with the peptide α4-vFLIP induced autophagy following poly(I:C) treatment, significantly abolishing lung inflammation and injury. Although there are other compounds to induce autophagy, α4-vFLIP had been shown to be potent, robust, and specific in inducing autophagy and could potentially be a promising therapeutic for ALI/ARDS.[24] We demonstrated that α4-vFLIP was able to induce autophagy in CD11c^{+} APCs and reduce inflammation. While targeting specific cell populations may be challenging, our

results do support an important role of autophagy in CD11c$^+$ APCs in modulating lung inflammation and injury in ALI/ARDS. Future studies are warranted to achieve targeted autophagy modulation and to evaluate the efficacy and safety of α4-vFLIP for use in a clinical setting. In conclusion, this study indicates that enhancing autophagy in CD11c$^+$ cells can be a promising targeted treatment that could alleviate and shorten the duration of ARDS, thus significantly decreasing the onset of complications that arise in patients experiencing ALI/ARDS induced by RNA viruses.

Limitations of the study

Our study clearly demonstrates a role for CD11c$^+$ APCs in ARDS and that modulating autophagy specifically in these cells can alleviate inflammation and injury. However, targeting these specific cells in mice and patients is challenging and warrants future studies. Our α4-vFLIP treatment in mice does induce autophagy overall. Therefore, we cannot exclude the possibility that increasing autophagy in CD11c$^-$ cells may also have an impact on lung inflammation and injury. We showed that CD11c$^+$ APCs are highly affected by treatment with α4-vFLIP (Figure 6B). Additionally, our Atg5 mice, which are autophagy deficient in CD11c$^+$ cells, demonstrated increased inflammation and injury upon poly(I:C) stimulation, and our Tfeb mice, which have constitutive autophagy induction specifically in CD11c$^+$ cells, showed attenuated inflammation and injury (Figures 3 and 4).

STAR★METHODS

Detailed methods are provided in the online version of this paper and include the following:

RESOURCE AVAILABILITY

Lead contact—Further information and requests for resources and reagents should be directed to and will be fulfilled by the lead contact, Dr. Omid Akbari (akbari@usc.edu)

All data reported in this paper will be shared by the lead contact upon request.

Materials availability—This study did not generate new unique reagents.

Data and code availability

- Bulk RNA-seq data have been deposited at GEO and are publicly available as of the date of publication. The accession number for the data is GEO: GSE227213.

- This paper does not report original code.

- Any additional information required to reanalyze the data reported in this paper is available from the lead contact upon request.

EXPERIMENTAL MODEL DETAILS

Mice—Wild-type (WT) C57BL/6, and CD11c-Cre mice were purchased from Jackson Laboratory (Bar Harbor, ME). *Atg5$^{flox/flox}$* and GFP-LC3 mice were a gift from Dr. Noboru Mizushima (Tokyo Medical and Dental University, Tokyo, Japan). *Tfeb$^{flox/flox}$* containing a flox/flox around a stop codon were a gift from Dr. Babak Razani (University of

Pittsburgh School of Medicine, Pittsburgh, PA). All transgenic mice were bred on a C57Bl/6 background. Six to eight-week-old aged- and sexed-matched mice were used in the study. *Atg5flox/flox* and *Tfebflox/flox* were bred with CD11c-Cre mice to produce Atg5-CD11c-Cre knockout mice (Atg5[KO]) and Tfeb-CD11c-Cre transgenic mice (Tfeb[TG]). Mice were bred in the animal facility of the Keck School of Medicine, University of Southern California (USC). All animal studies were approved by the USC institutional Animal Care and Use Committee (IACUC) and conducted in accordance with the USC Department of Animal Resources' guidelines.

Cell culture—THP-1-DifluohLC3 cells (InvivoGen, San Diego, CA) were cultured in Roswell Park Memorial Institute (RPMI) 1640 medium (Corning, Manassas, VA) supplemented with 10% fetal bovine serum (FBS) (Omega Scientific, Tarzana, CA), 1% penicillin-streptomycin and zeocin (100 μg/mL). Cells were stimulated with 100mM of phorbol-12-myristate-13-acetate (PMA) (Sigma Aldrich, St. Louis, MO) for 3 days to induce THP-1 differentiation into adherent macrophage-like cells. Cells were allowed a 2-h rest without PMA and then stimulated with 20 μg/mL of polyinosinic-polycytidylic acid (Poly(I:C)) high molecular weight (InvivoGen, San Diego, CA). Cells were treated with either α4-vFLIP peptide (30μM), TAT peptide (30μM) or rapamycin (500nM) for 24 h. Cells were collected and GFP and RFP mean fluorescence intensity (MFI) were measured on a BD FACSCanto II (BD Biosciences).

METHOD DETAILS

Poly(I:C) administration—Mice were intranasally (*i.n.*) challenged for 3 consecutive days with 40 μg polyinosinic-polycytidylic acid (Poly(I:C)) high molecular weight in 40 μL PBS (InvivoGen, San Diego, CA) to induce ALI/ARDS. AHR was measured 24 h after the last treatment and mice were euthanized for further downstream analysis. For the α4-viral Fas-associated death domain-like interleukin-1β-converting enzyme-inhibitory protein (α4-vFLIP) experiments, mice were challenged with poly(I:C) *i.n.* and treated intraperitoneal (*i.p.*) with 300mg α4-vFLIP or *trans*-activator of transcription (TAT) peptide for 3 consecutive days.

Measurement of airway hyperreactivity (AHR)—Mice were intranasally challenged with Poly(I:C) or PBS as shown in the experimental schemes. Lung function was assessed by direct measurement of lung resistance and dynamic compliance (cDyn) in restrained, tracheostomized, and mechanically ventilated mice using the FinePointe RC system (Buxco Research Systems) under general anesthesia as previously described.[48] Mice were sequentially challenged with aerosolized PBS (baseline), followed by increasing doses of methacholine ranging from 5 to 80 mg/mL. Maximum lung resistance and minimum compliance values were recorded during a 3-min period after each methacholine challenge. AHR data were analyzed by repeated measurements of a general linear model.

Tissue processing and flow cytometry—Following AHR measurements, the trachea was cannulated and the bronchoalveolar lavage (BAL) fluid was collected. Briefly, lungs were washed three times with 1mL of ice-cold PBS. BAL supernatant was collected to quantify protein concentration using Pierce BCA Protein Assay Kit (Thermo

Fisher Scientific, Waltham, MA) and cytokines using mouse anti-virus response panel LEGENDplex Multiplex Assay (Biolegend) according to manufacturer's instructions. Lungs were collected and minced into small pieces and subsequently incubated in type IV collagenase (400 U/ml; Worthington Biochemicals) at 37°C for 60 min. After digestion, the lung digest was passed through a 70-μm cell strainer (Falcon) to create a single cell suspension. Cells were washed with PBS and centrifuged at $500 \times g$ for 6 min at 4°C. In order to exclude and lyse the red blood cells (RBCs), the pellet was resuspended in 1X RBC lysis buffer (Biolegend, San Diego) and incubated at room temperature for 5 min. The reaction was terminated by washing the cells with PBS. The remaining pellet was then further prepared for flow cytometry. Immune cell populations were identified in BAL and lung using the following antibodies: APC-Cy7 anti-mouse CD45 (clone 30-F11; BioLegend), FITC anti-mouse CD45 (clone 30-F11, eBioscience) PE-Cy7 anti-mouse CD11c (clone HL3; BD Bioscences), PerCP/Cyanine5.5 anti-mouse CD11c (clone N418, BioLegend), PE anti-mouse Siglec-F (clone E50-2440; BD Biosciences), PerCP/Cyanine5.5 anti-mouse CD11b (clone M1/70; BioLegend), BV421 anti-mouse/human CD11b (clone M1/70, BioLegend), APC anti-mouse Gr-1 (clone RB6-8C5; BioLegend), BV510 anti-mouse CD19 (clone 6D5; BioLegend), PerCP/Cyanine5.5 anti-mouse CD3 (clone 17A2; BioLegend), PE anti-mouse CD64 (clone X54-5/7.1, BioLegend), APC-Cyanine7 anti-mouse Ly-6C (clone HK1.4, BioLegend), APC anti-mouse CD163 (clone S15049, BioLegend), PerCP/Cyanine5.5 anti-mouse CD36 (clone HM3.6, BioLegend), FITC anti-mouse CD206 (clone C068C2, BioLegend), BV421 anti-mouse CD86 (GL-1, BioLegend), BV510 anti-mouse I-A/I-E (MHC-II) (clone M5/114.15.2, BioLegend), and anti-mouse Fc-block (2.4G2. BioXcell). A 1:500 dilution was used for all antibodies. CountBright Absolute Count Beads (Thermo Fisher Scientific, Waltham, MA) were used to count BAL and lung immune cell. Acquisition was performed on a BD FACSCanto II (BD Biosciences) using the BD FACSDiva software v8.0.1. Data were analyzed with FlowJo software (TreeStar) version 10.

Lung histology—After euthanasia, mice lungs were harvested and fixed in 10% buffered formalin. After overnight staining, lungs were processed for histology. The lungs were embedded in paraffin and cut into 4mm sections. Tissue sections were routinely stained with hematoxylin and eosin (H&E). Images were acquired on a Keyence BZ-X700 (Keyence, Itasca, IL) using a 40x objective and BZ-X Viewer 01.03.01.01 and analyzed with ImageJ (NIH & LOC).

Lung permeability assay—Mice were treated with poly(I:C) as previously mentioned and lung permeability was determined by fluorescein isothicyanate-dextran (FITC-Dextran) leakage from the airways into the blood. On Day 4, mice were instilled *i.n.* with 10mg of FITC-Dextran per kg mouse dissolved in sterile PBS under general anesthesia (Sigma, St. Louis, MO). After 30 min, mice were sacrificed, and blood was collected by cardiac puncture. Blood was treated with 10uL of EDTA and centrifuged at 4,000 rpm for 4 min at 4°C. The plasma was used to measure the fluorescence intensity at an excitation wavelength of 485 nm and an emission wavelength of 528nm using a Synergy 2 microplate reader (Biotek). The experiment was performed 3 times. Experiments were repeated three times.

Confocal laser scanning microscopy—THP1-Difluo hLC3 cells were seeded on coverslips and cultured and treated as previously described above. Cells were washed with PBS and then fixed with 4% paraformaldehyde (20 min at RT). After fixation, cells were extensively washed with PBS and then mounted using ProLong Diamond Antifade Mountant with DAPI (4′, 6′-diamidino-2-phenylindole) (Invitrogen). Confocal images were acquired using a Nikon Eclipse C1 laser-scanning microscope (Nikon, PA), fitted with a 60× Nikon objective (PL APO, 1.4NA), and NIS Elements AR 5.41.02 Nikon imaging software. Approximately 10–20 cells were imaged per group. Images were collected at 512×512 pixel resolution.

Immunoblotting—For immunoblotting, sorted CD11c$^+$ and CD11c$^-$ cells from the lungs of C57Bl/6 mice treated with poly(I:C) or PBS were lysed in RIPA lysis buffer (EMD Millipore) supplemented with protease inhibitor cocktail (Roche) for 30 min. Lysates were centrifuged (13,000 × g at 4°C for 15 min) and supernatants were collected. Protein concentrations were determined using the Pierce BCA Protein Assay Kit (Thermo Scientific) and samples adjusted to the same concentration. The adjusted protein eluates were mixed with 6X Laemmli SDS sample buffer (Bioland Scientific) and heated at 95°C for 5 min. Protein eluates were resolved by SDS-PAGE and transferred to a PVDF membrane (BioRad). Membranes were blocked with 5% BSA and probed with LC3B (1:250, Cell Signaling Technology), p62 (1:250, Cell Signaling Technology) and β-actin (1:1000, Santa Cruz Biotechnology) at 4°C overnight. Membranes were incubated with horseradish peroxidase (HRP) conjugated goat secondary antibodies (1:1000, Invitrogen). Immunodetection was achieved by ProSignal Pico Spray (Genesee Scientific) and detected on a ChemiDoc Imaging System (BioRad).

RNA-sequencing (RNAseq)—Total RNA was isolated from CD11c$^+$ cells sorted from Poly(I:C) treated mice was isolated using RNeasy Mini Kit (Qiagen). In total, 10 ng of input RNA was used to produce cDNA for downstream library preparation. Samples were sequenced on a NextSeq 500 (Illumina) system. Raw reads were aligned, normalized, and further analyzed using **Partek Flow, version 10.0** Copyright; Partek Inc. Normalized read counts were tested for differential expression using Partek's Gene-Specific Analysis (GSA) algorithm. The data discussed in this publication has been deposited in NCBI's Gene Expression Omnibus and are accessible through GEO series accession number GSE227213.

QUANTIFICATION AND STATISTICAL ANALYSIS

Data are representative of at least two independent experiments and are presented as means ± SEM (except for RNAseq). Two-tailed Student's t-test was applied for comparisons between 2 groups. For multigroup comparisons, we used one-way ANOVA with the Tukey post hoc test or two-way ANOVA. Data were analyzed with Prism 7 Software (GraphPad Software Inc.). Error bars represent standard error of the mean. p value < 0.05 was considered to denote statistical significance ($*p < 0.05$, $**p < 0.01$, $***p < 0.001$).

Supplementary Material

Refer to Web version on PubMed Central for supplementary material.

ACKNOWLEDGMENTS

INCLUSION AND DIVERSITY

We support inclusive, diverse, and equitable conduct of research.

REFERENCES

1. Matthay MA, Zemans RL, Zimmerman GA, Arabi YM, Beitler JR, Mercat A, Herridge M, Randolph AG, and Calfee CS (2019). Acute respiratory distress syndrome. Nat. Rev. Dis. Primers 5, 18. 10.1038/s41572-019-0069-0. [PubMed: 30872586]

2. Wheeler AP, and Bernard GR (2007). Acute lung injury and the acute respiratory distress syndrome: a clinical review. Lancet 369, 1553–1564. 10.1016/S0140-6736(07)60604-7. [PubMed: 17482987]

3. Matthay MA, Ware LB, and Zimmerman GA (2012). The acute respiratory distress syndrome. J. Clin. Invest. 122, 2731–2740. 10.1172/JCI60331. [PubMed: 22850883]

4. Matute-Bello G, Downey G, Moore BB, Groshong SD, Matthay MA, Slutsky AS, and Kuebler WM; Acute Lung Injury in Animals Study Group (2011). An official American Thoracic Society workshop report: features and measurements of experimental acute lung injury in animals. Am. J. Respir. Cell Mol. Biol. 44, 725–738. 10.1165/rcmb.2009-0210ST. [PubMed: 21531958]

5. Huang LY, Stuart C, Takeda K, D'Agnillo F, and Golding B (2016). Poly(I:C) Induces Human Lung Endothelial Barrier Dysfunction by Disrupting Tight Junction Expression of Claudin-5. PLoS One 11, e0160875. 10.1371/journal.pone.0160875. [PubMed: 27504984]

6. Gan T, Yang Y, Hu F, Chen X, Zhou J, Li Y, Xu Y, Wang H, Chen Y, and Zhang M (2018). TLR3 Regulated Poly I:C-Induced Neutrophil Extracellular Traps and Acute Lung Injury Partly Through p38 MAP Kinase. Front. Microbiol. 9, 3174. 10.3389/fmicb.2018.03174. [PubMed: 30622526]

7. Chun CD, Liles WC, Frevert CW, Glenny RW, and Altemeier WA (2010). Mechanical ventilation modulates Toll-like receptor-3-induced lung inflammation via a MyD88-dependent, TLR4-independent pathway: a controlled animal study. BMC Pulm. Med. 10, 57. 10.1186/1471-2466-10-57. [PubMed: 21092115]

8. Gao X, Chan PKS, Lui GCY, Hui DSC, Chu IMT, Sun X, Tsang MSM, Chan BCL, Lam CWK, and Wong CK (2021). Interleukin-38 ameliorates poly(I:C) induced lung inflammation: therapeutic implications in respiratory viral infections. Cell Death Dis. 12, 53. 10.1038/s41419-020-03283-2. [PubMed: 33414457]

9. Chen X, Tang J, Shuai W, Meng J, Feng J, and Han Z (2020). Macrophage polarization and its role in the pathogenesis of acute lung injury/acute respiratory distress syndrome. Inflamm. Res. 69, 883–895. 10.1007/s00011-020-01378-2. [PubMed: 32647933]

10. Aggarwal NR, King LS, and D'Alessio FR (2014). Diverse macrophage populations mediate acute lung inflammation and resolution. Am. J. Physiol. Lung Cell Mol. Physiol. 306, L709–L725. 10.1152/ajplung.00341.2013. [PubMed: 24508730]

11. Painter JD, Galle-Treger L, and Akbari O (2020). Role of Autophagy in Lung Inflammation. Front. Immunol. 11, 1337. 10.3389/fimmu.2020.01337. [PubMed: 32733448]

12. Levine B, Mizushima N, and Virgin HW (2011). Autophagy in immunity and inflammation. Nature 469, 323–335. 10.1038/nature09782. [PubMed: 21248839]

13. Levine B, and Kroemer G (2008). Autophagy in the pathogenesis of disease. Cell 132, 27–42. 10.1016/j.cell.2007.12.018. [PubMed: 18191218]

14. Ahmad L, Mostowy S, and Sancho-Shimizu V (2018). Autophagy-Virus Interplay: From Cell Biology to Human Disease. Front. Cell Dev. Biol. 6, 155. 10.3389/fcell.2018.00155. [PubMed: 30510929]

15. Germic N, Frangez Z, Yousefi S, and Simon HU (2019). Regulation of the innate immune system by autophagy: monocytes, macrophages, dendritic cells and antigen presentation. Cell Death Differ. 26, 715–727. 10.1038/s41418-019-0297-6. [PubMed: 30737475]

16. Mizushima N, and Levine B (2020). Autophagy in Human Diseases. N. Engl. J. Med. 383, 1564–1576. 10.1056/NEJMra2022774. [PubMed: 33053285]

17. Galle-Treger L, Helou DG, Quach C, Howard E, Hurrell BP, Muench GRA, Shafiei-Jahani P, Painter JD, Iorga A, Dara L, et al. (2022). Autophagy impairment in liver CD11c + cells promotes non-alcoholic fatty liver disease through production of IL-23. Nat. Commun. 13, 1440. 10.1038/s41467-022-29174-y. [PubMed: 35301333]

18. Quach C, Song Y, Guo H, Li S, Maazi H, Fung M, Sands N, O'Connell D, Restrepo-Vassalli S, Chai B, et al. (2019). A truncating mutation in the autophagy gene UVRAG drives inflammation and tumorigenesis in mice. Nat. Commun. 10, 5681. 10.1038/s41467-019-13475-w. [PubMed: 31831743]

19. Ganesan R, Hos NJ, Gutierrez S, Fischer J, Stepek JM, Daglidu E, Krönke M, and Robinson N (2017). Salmonella Typhimurium disrupts Sirt1/AMPK checkpoint control of mTOR to impair autophagy. PLoS Pathog. 13, e1006227. 10.1371/journal.ppat.1006227. [PubMed: 28192515]

20. Zubova SG, Suvorova II, and Karpenko MN (2022). Macrophage and microglia polarization: focus on autophagy-dependent reprogramming. Front. Biosci. 14, 3. 10.31083/j.fbs1401003.

21. Suzuki Y, Maazi H, Sankaranarayanan I, Lam J, Khoo B, Soroosh P, Barbers RG, James Ou JH, Jung JU, and Akbari O (2016). Lack of autophagy induces steroid-resistant airway inflammation. J. Allergy Clin. Immunol. 137, 1382–1389.e9. 10.1016/j.jaci.2015.09.033. [PubMed: 26589586]

22. Sergin I, Evans TD, Zhang X, Bhattacharya S, Stokes CJ, Song E, Ali S, Dehestani B, Holloway KB, Micevych PS, et al. (2017). Exploiting macrophage autophagy-lysosomal biogenesis as a therapy for atherosclerosis. Nat. Commun. 8, 15750. 10.1038/ncomms15750. [PubMed: 28589926]

23. Javaheri A, Bajpai G, Picataggi A, Mani S, Foroughi L, Evie H, Kovacs A, Weinheimer CJ, Hyrc K, Xiao Q, et al. (2019). TFEB activation in macrophages attenuates postmyocardial infarction ventricular dysfunction independently of ATG5-mediated autophagy. JCI Insight 4, e127312. 10.1172/jci.insight.127312. [PubMed: 31672943]

24. Lee JS, Li Q, Lee JY, Lee SH, Jeong JH, Lee HR, Chang H, Zhou FC, Gao SJ, Liang C, and Jung JU (2009). FLIP-mediated autophagy regulation in cell death control. Nat. Cell Biol. 11, 1355–1362. 10.1038/ncb1980. [PubMed: 19838173]

25. Klionsky DJ, Abdel-Aziz AK, Abdelfatah S, Abdellatif M, Abdoli A, Abel S, Abeliovich H, Abildgaard MH, Abudu YP, Acevedo-Arozena A, et al. (2021). Guidelines for the use and interpretation of assays for monitoring autophagy. Autophagy 17 (4th edition), 1–382, 17. 10.1080/15548627.2020.1797280.

26. Mizushima N, Yoshimori T, and Levine B (2010). Methods in mammalian autophagy research. Cell 140, 313–326. 10.1016/j.cell.2010.01.028. [PubMed: 20144757]

27. Yoshii SR, and Mizushima N (2017). Monitoring and Measuring Autophagy. Int. J. Mol. Sci. 18, 1865. 10.3390/ijms18091865. [PubMed: 28846632]

28. Levine B, and Kroemer G (2019). Biological Functions of Autophagy Genes: A Disease Perspective. Cell 176, 11–42. 10.1016/j.cell.2018.09.048. [PubMed: 30633901]

29. Hara T, Nakamura K, Matsui M, Yamamoto A, Nakahara Y, Suzuki-Migishima R, Yokoyama M, Mishima K, Saito I, Okano H, and Mizushima N (2006). Suppression of basal autophagy in neural cells causes neurodegenerative disease in mice. Nature 441, 885–889. 10.1038/nature04724. [PubMed: 16625204]

30. Shoji-Kawata S, Sumpter R, Leveno M, Campbell GR, Zou Z, Kinch L, Wilkins AD, Sun Q, Pallauf K, MacDuff D, et al. (2013). Identification of a candidate therapeutic autophagy-inducing peptide. Nature 494, 201–206. 10.1038/nature11866. [PubMed: 23364696]

31. Starkhammar M, Kumlien Georén S, Swedin L, Dahlén SE, Adner M, and Cardell LO (2012). Intranasal administration of poly(I:C) and LPS in BALB/c mice induces airway hyperresponsiveness and inflammation via different pathways. PLoS One 7, e32110. 10.1371/journal.pone.0032110. [PubMed: 22355412]

32. Rittirsch D, Flierl MA, Day DE, Nadeau BA, McGuire SR, Hoesel LM, Ipaktchi K, Zetoune FS, Sarma JV, Leng L, et al. (2008). Acute lung injury induced by lipopolysaccharide is independent of complement activation. J. Immunol. 180, 7664–7672. 10.4049/jimmunol.180.11.7664. [PubMed: 18490769]

33. Ali H, Khan A, Ali J, Ullah H, Khan A, Ali H, Irshad N, and Khan S (2020). Attenuation of LPS-induced acute lung injury by continentalic acid in rodents through inhibition of inflammatory mediators correlates with increased Nrf2 protein expression. BMC Pharmacol. Toxicol. 21, 81. 10.1186/s40360-020-00458-7. [PubMed: 33239093]

34. Kosyreva A, Dzhalilova D, Lokhonina A, Vishnyakova P, and Fatkhudinov T (2021). The Role of Macrophages in the Pathogenesis of SARS-CoV-2-Associated Acute Respiratory Distress Syndrome. Front. Immunol. 12, 682871. 10.3389/fimmu.2021.682871. [PubMed: 34040616]

35. Park WY, Goodman RB, Steinberg KP, Ruzinski JT, Radella F, Park DR, Pugin J, Skerrett SJ, Hudson LD, and Martin TR (2001). Cytokine balance in the lungs of patients with acute respiratory distress syndrome. Am. J. Respir. Crit. Care Med. 164, 1896–1903. 10.1164/ajrccm.164.10.2104013. [PubMed: 11734443]

36. Liu K, Zhao E, Ilyas G, Lalazar G, Lin Y, Haseeb M, Tanaka KE, and Czaja MJ (2015). Impaired macrophage autophagy increases the immune response in obese mice by promoting proinflammatory macrophage polarization. Autophagy 11, 271–284. 10.1080/15548627.2015.1009787. [PubMed: 25650776]

37. Huang X, Xiu H, Zhang S, and Zhang G (2018). The Role of Macrophages in the Pathogenesis of ALI/ARDS. Mediators Inflamm. 2018, 1264913. 10.1155/2018/1264913. [PubMed: 29950923]

38. Hurrell BP, Schuster S, Grün E, Coutaz M, Williams RA, Held W, Malissen B, Malissen M, Yousefi S, Simon HU, et al. (2015). Rapid Sequestration of Leishmania mexicana by Neutrophils Contributes to the Development of Chronic Lesion. PLoS Pathog. 11, e1004929. 10.1371/journal.ppat.1004929. [PubMed: 26020515]

39. Shi C, and Pamer EG (2011). Monocyte recruitment during infection and inflammation. Nat. Rev. Immunol. 11, 762–774. 10.1038/nri3070. [PubMed: 21984070]

40. Yang N, and Shen HM (2020). Targeting the Endocytic Pathway and Autophagy Process as a Novel Therapeutic Strategy in COVID-19. Int. J. Biol. Sci. 16, 1724–1731. 10.7150/ijbs.45498. [PubMed: 32226290]

41. Chang CP, Su YC, Hu CW, and Lei HY (2013). TLR2-dependent selective autophagy regulates NF-κB lysosomal degradation in hepatoma-derived M2 macrophage differentiation. Cell Death Differ. 20, 515–523. 10.1038/cdd.2012.146. [PubMed: 23175187]

42. Das LM, Binko AM, Traylor ZP, Peng H, and Lu KQ (2019). Vitamin D improves sunburns by increasing autophagy in M2 macrophages. Autophagy 15, 813–826. 10.1080/15548627.2019.1569298. [PubMed: 30661440]

43. Yang Y, Wei S, Chu K, Li Q, Zhou Y, Ma Y, Xue L, Tian H, and Tao S (2021). Upregulation of autophagy in M2 macrophage by vitamin D alleviates crystalline silica-induced pulmonary inflammatory damage. Ecotoxicol. Environ. Saf. 225, 112730. 10.1016/j.ecoenv.2021.112730. [PubMed: 34478973]

44. Nosaka N, Martinon D, Moreira D, Crother TR, Arditi M, and Shimada K (2020). Autophagy Protects Against Developing Increased Lung Permeability and Hypoxemia by Down Regulating Inflammasome Activity and IL-1β in LPS Plus Mechanical Ventilation-Induced Acute Lung Injury. Front. Immunol. 11, 207. 10.3389/fimmu.2020.00207. [PubMed: 32117318]

45. Ichikawa A, Kuba K, Morita M, Chida S, Tezuka H, Hara H, Sasaki T, Ohteki T, Ranieri VM, dos Santos CC, et al. (2013). CXCL10-CXCR3 enhances the development of neutrophil-mediated fulminant lung injury of viral and nonviral origin. Am. J. Respir. Crit. Care Med. 187, 65–77. 10.1164/rccm.201203-0508OC. [PubMed: 23144331]

46. Williams AE, José RJ, Mercer PF, Brealey D, Parekh D, Thickett DR, O'Kane C, McAuley DF, and Chambers RC (2017). Evidence for chemokine synergy during neutrophil migration in ARDS. Thorax 72, 66–73. 10.1136/thoraxjnl-2016-208597. [PubMed: 27496101]

47. Lang S, Li L, Wang X, Sun J, Xue X, Xiao Y, Zhang M, Ao T, and Wang J (2017). CXCL10/IP-10 Neutralization Can Ameliorate Lipopolysaccharide-Induced Acute Respiratory Distress Syndrome in Rats. PLoS One 12, e0169100. 10.1371/journal.pone.0169100. [PubMed: 28046003]

48. Shafiei-Jahani P, Helou DG, Hurrell BP, Galle-Treger L, Howard E, Quach C, Painter JD, Fung M, Lo R, Allayee H, and Akbari O (2021). CD52-targeted depletion by Alemtuzumab ameliorates allergic airway hyperreactivity and lung inflammation. Mucosal Immunol. 14, 899–911. 10.1038/s41385-021-00388-5. [PubMed: 33731828]

Highlights

- Poly(I:C) impairs autophagy in CD11c$^+$ APCs

- Autophagy deficiency in CD11c$^+$ APCs exacerbates lung inflammation and injury

- Autophagy induction in CD11c$^+$ APCs attenuates lung inflammation and injury
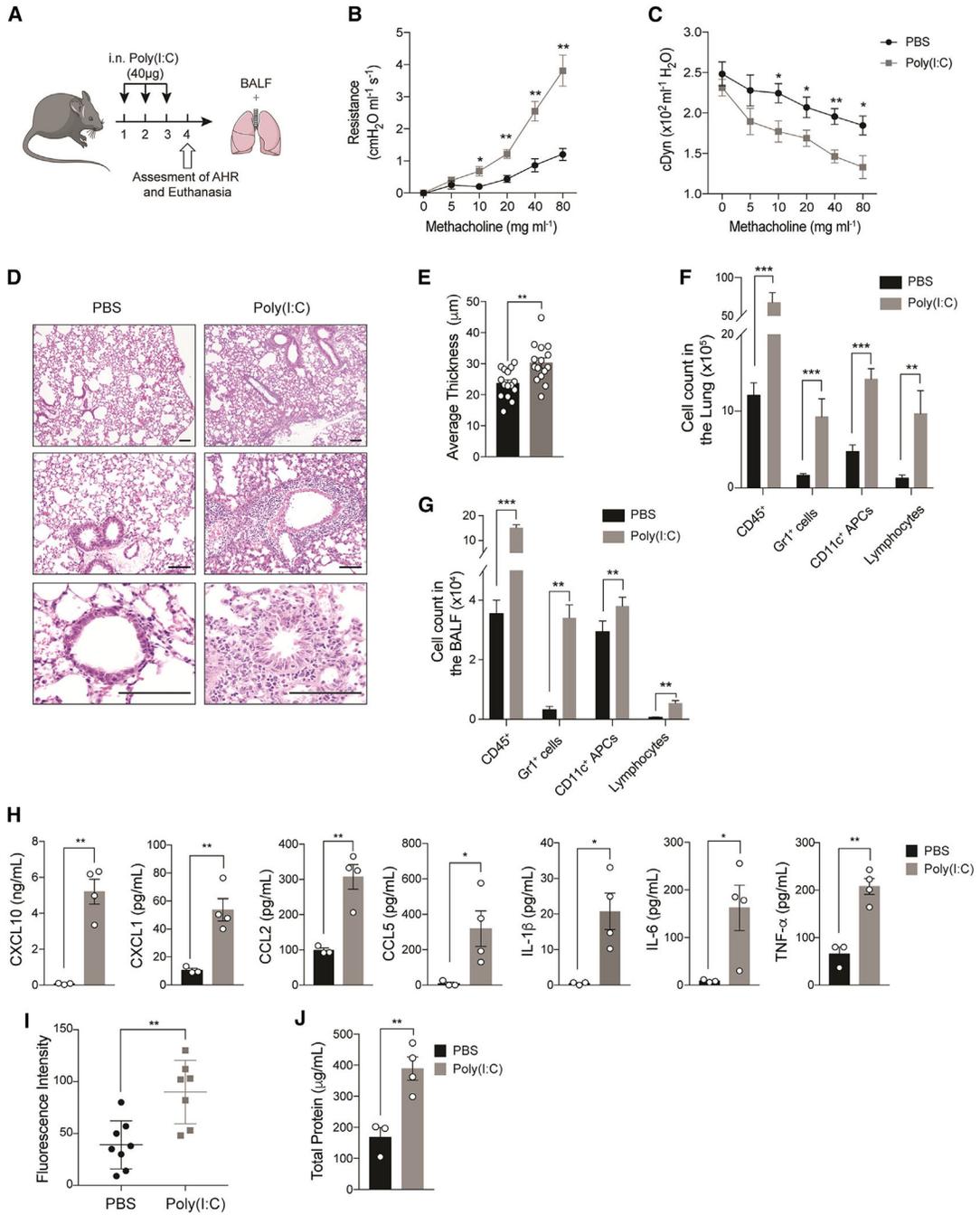
Figure 1. Poly(I:C) stimulation induces lung inflammation and injury

(A) C57BL/6 mice were intranasally (i.n.) challenged with 40 μg poly(I:C) for 3 consecutive days, and on the fourth day, AHR was measured and BALF and lungs collected for analysis.

(B and C) Lung resistance (B) and dynamic compliance (C) were measured in tracheostomized ventilated mice (n = 5–6 mice per group).

(D) Hematoxylin and eosin (H&E) staining of lung sections (scale bar: 100 μm).

(E) Average airway thickness.

(F and G) Total number of immune cells in the (F) BALF and in the (G) lungs.

(H) Levels of pro-inflammatory cytokines and chemokines in the BALF quantified by using BioLegend LEGENDplex bead-based immunoassay.

(I) FITC-dextran fluorescence intensity.

(J) Protein concentration in the BALF.

Data are represented as means ± SEM (unpaired Student's t test). ns, not significant, *p < 0.05; **p < 0.01; ***p < 0.001.

See also Figure S1.

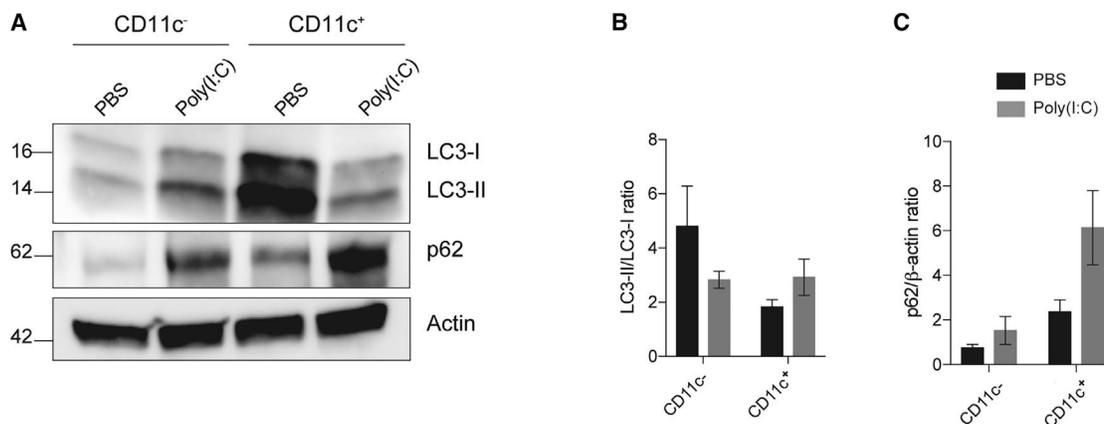**Figure 2. Poly(I:C) stimulation downregulates autophagy in CD11c⁺ APCs**

(A) Representative western blot of LC3-I and LC3-II and p62 levels in CD11c⁺ and CD11c⁻ cells sorted from the lungs of C57BL/6 mice (n = 7 mice per group) treated with 40 μg poly(I:C) or PBS.

(B) Visual representation of the densiometric quantification of LC3-II/LC3-I ratio.

(C) Visual representation of the densiometric quantification of p62/β-actin ratio in CD11c⁺ cells only.

Data are represented as means ± SEM (unpaired Student's t test). ns, not significant, *p < 0.05; **p < 0.01; ***p < 0.001, ****p < 0.0001.
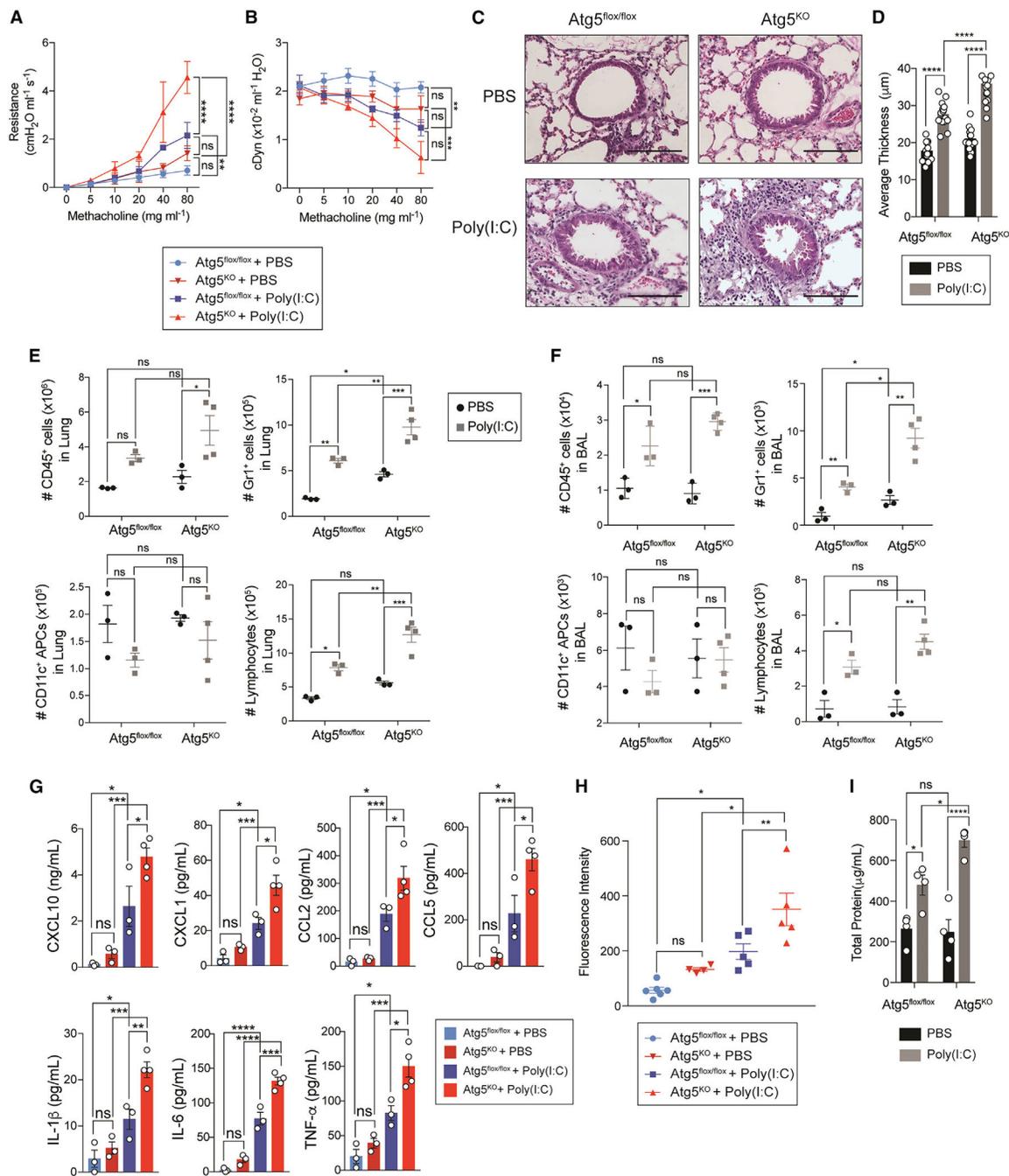
See also Figure S2.

Figure 3. Lack of autophagy in pulmonary CD11c^{+} APCs exacerbates lung inflammation and injury

Atg5[flox/flox] and Atg5[KO] mice were i.n. challenged with 40 μg poly(I:C) or PBS for 3 consecutive days, and on the fourth day, AHR was measured and BALF and lungs collected for analysis (n = 3–4 mice per group).

(A and B) Lung resistance (A) and dynamic compliance (B) were measured in tracheostomized ventilated mice (n = 3 mice per group).

(C) H&E staining of lung sections (scale bar: 100 μm).

(D) Average airway thickness.

(E and F) Total number of immune cells in the (E) BALF and in the (F) lungs.

(G) Levels of pro-inflammatory cytokines and chemokines in the BALF quantified by using BioLegend LEGENDplex bead-base immunoassay.

(H) FITC-dextran fluorescence intensity.

(I) Protein concentration in the BALF.

Data are represented as means ± SEM (two-way ANOVA). ns, not significant, $*p < 0.05$; $**p < 0.01$; $***p < 0.001$.
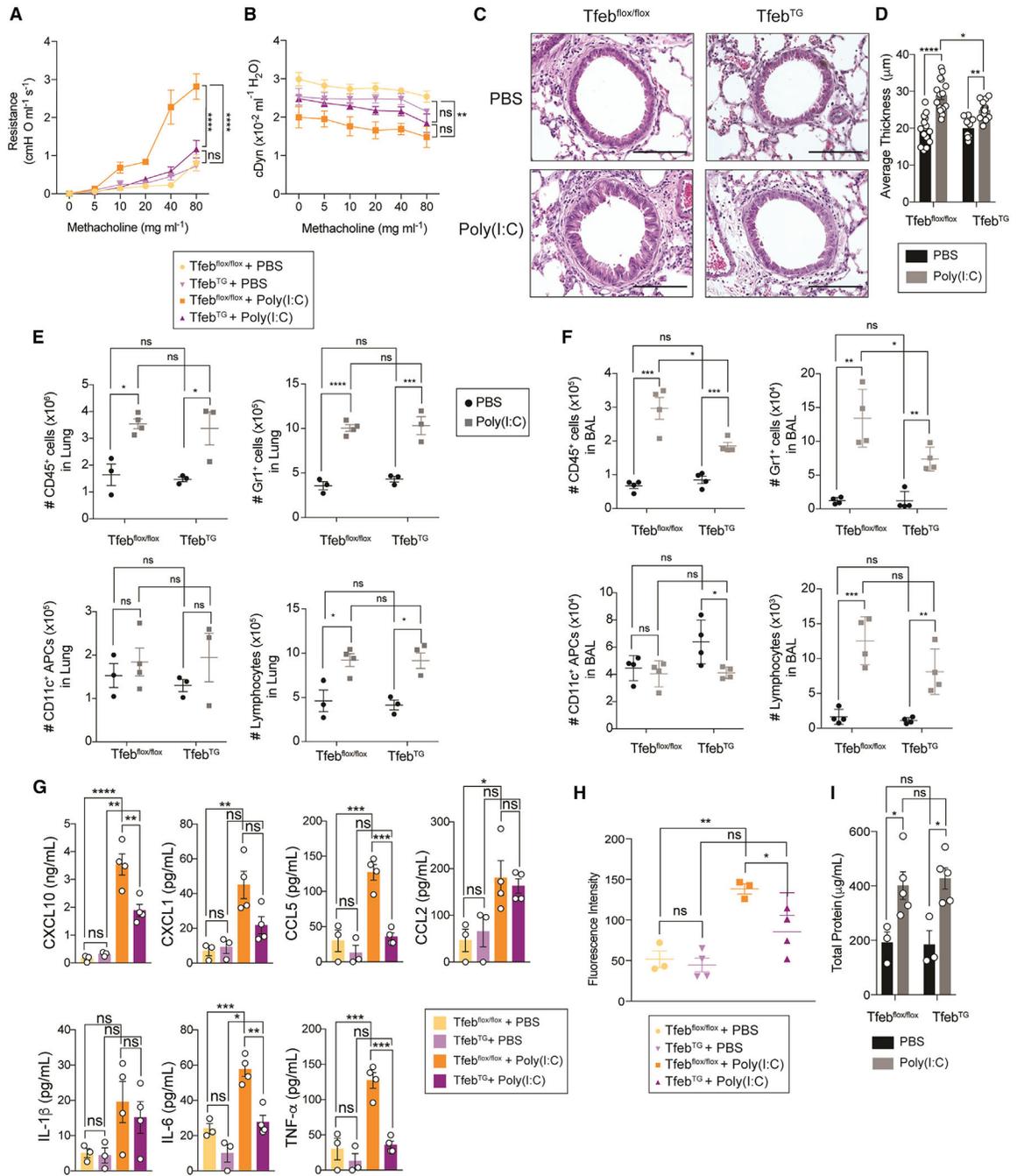
See also Figure S3.

Figure 4. Autophagy induction in pulmonary CD11c$^+$ APCs attenuates lung inflammation and prevents lung injury

TFEB$^{flox/flox}$ and Tfeb^{TG} mice were i.n. challenged with 40 μg poly(I:C) or PBS for 3 consecutive days, and on the fourth day, AHR was measured and BALF and lungs collected for analysis.

(A and B) Lung resistance (A) and dynamic compliance (B) were measured in tracheostomized ventilated mice (n = 3–6 mice per group).

(C) H&E staining of lung sections (scale bar: 100 μm).

(D) Average airway thickness.

(E and F) Total number of immune cells in the (E) BALF and in the (F) lungs.

(G) Levels of pro-inflammatory cytokines and chemokines in the BALF quantified by using BioLegend LEGENDplex bead-base immunoassay.

(H) FITC-dextran fluorescence intensity.

(I) Protein concentration in the BALF.

Data are represented as means ± SEM (two-way ANOVA). ns, not significant, *p < 0.05; **p < 0.01; ***p < 0.001.
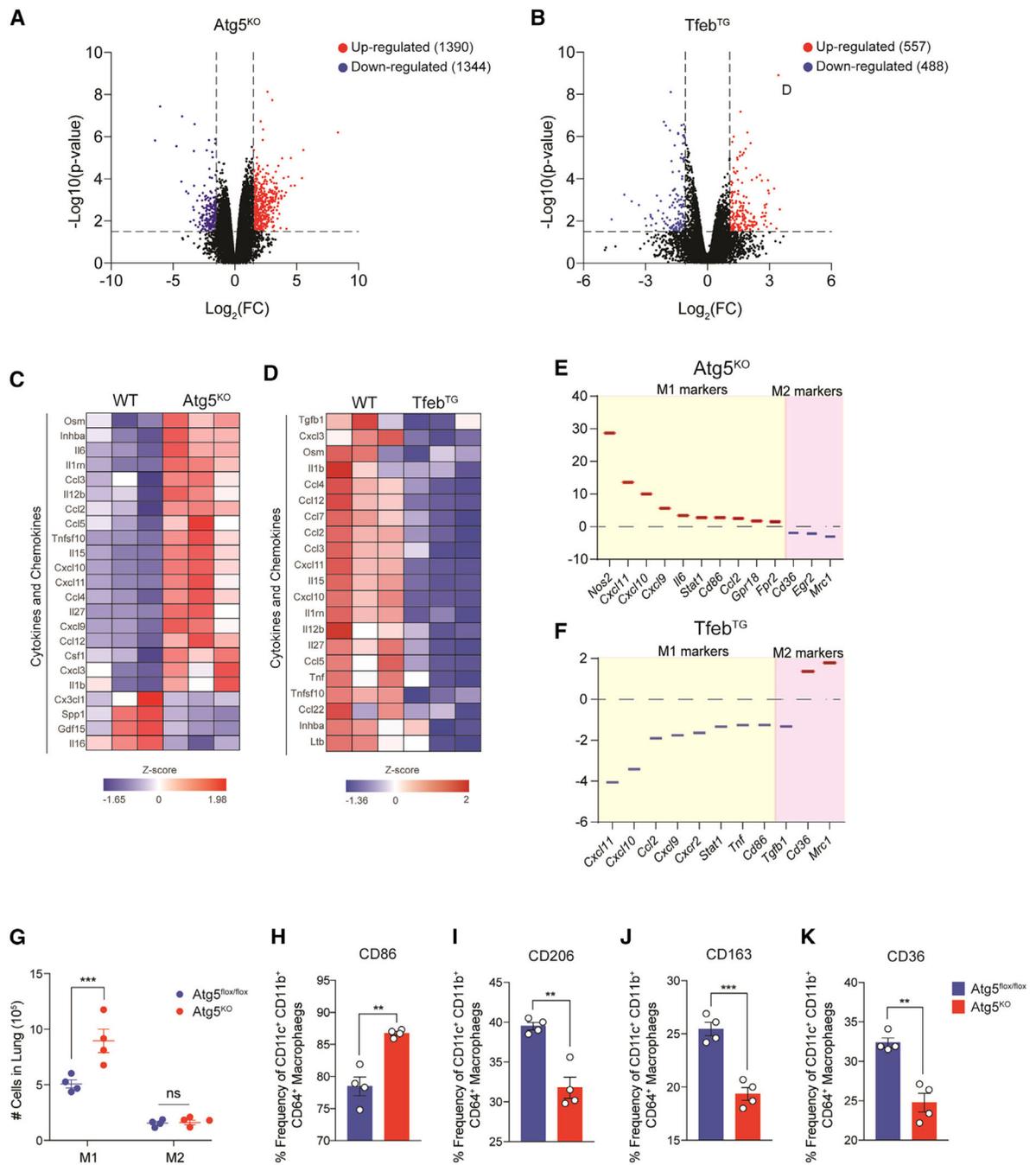
See also Figure S4.

Figure 5. A lack of autophagy significantly impacts gene expression of pro-inflammatory cytokines

(A) Volcano plot of differentially expressed genes in poly(I:C)-treated Atg5^KO vs. Atg5^flox/flox mice.

(B) Volcano plot of differentially expressed genes in poly(I:C)-treated Tfeb^TG vs. Tfeb^flox/flox mice.

(C) Heatmap representation of cytokines significantly modulated in poly(I:C)-treated Atg5^KO mice.

(D) Heatmap representation of cytokines significantly modulated in poly(I:C)-treated Tfeb^{TG} mice. n = 3 mice per group.

(E and F) The regulation of genes encoding for relevant M1/M2 markers represented as fold change in poly(I:C)-treated Atg5^{KO} vs. Atg5$^{flox/flox}$ control mice and in (F) Tfeb^{TG} vs. Tfeb$^{flox/flox}$ control mice.

(G) The number of M1 and M2 macrophages in the lungs of Atg5$^{flox/flox}$ and Atg5^{KO} mice challenged with poly(I:C).

(H–K) Frequency of CD11c$^+$ CD11b$^+$ CD64$^+$ macrophages expressing (H) CD86, (I) CD206, (J) CD163, and (K) CD36.

Data are represented as means ± SEM (two-way ANOVA). ns, not significant, *p < 0.05; **p < 0.01; ***p < 0.001.
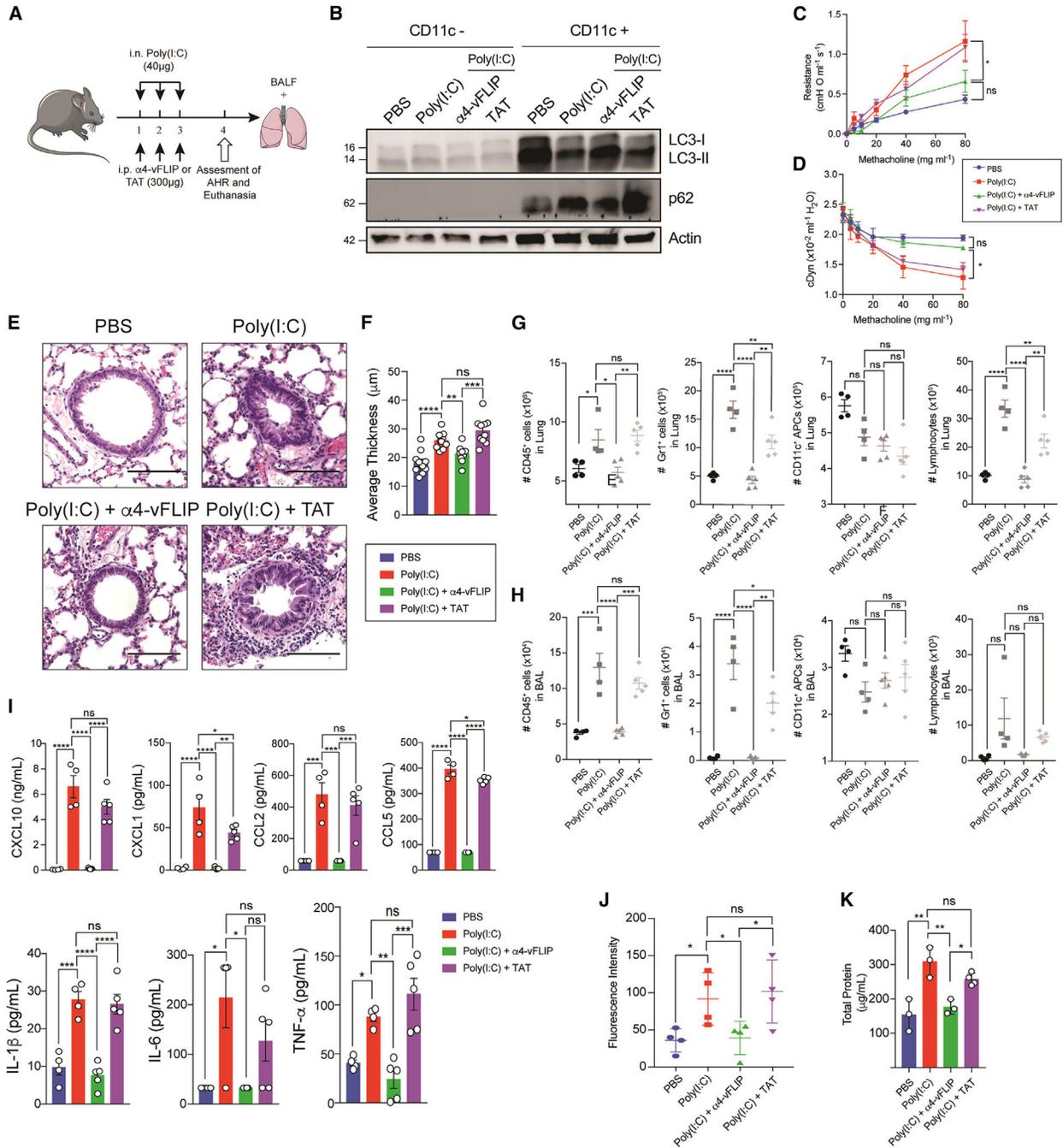
See also Figure S5.

Figure 6. Use of an autophagy inducer, α4-vFLIP, ameliorates lung inflammation and injury

(A) C57BL/6 mice were i.n. challenged with 40 μg poly(I:C) for 3 consecutive days in the morning followed by intraperitoneal (i.p.) injection of vFLIP (300 mg per mouse) or control peptide, TAT, in the evening. On the fourth day, AHR was measured and BALF and lungs collected for analysis.

(B) Western blot analysis of LC3-I and LC3-II and p62 levels in CD11c^{+} and CD11c^{−} cells sorted from the lungs of C57BL/6 mice treated with PBS, poly(I:C) only, poly(I:C) + α4-vFLIP, or poly(I:C) + TAT.

(C and D) Lung resistance (C) and dynamic compliance (D) were measured in tracheostomized ventilated mice (n = 3–6 mice per group).

(E) H&E staining of lung sections (scale bar: 100 μm).

(F) Average airway thickness.

(G and H) Total number of immune cells in the (G) BALF and in the (H) lungs.

(I) Levels of pro-inflammatory cytokines and chemokines in the BALF quantified by using BioLegend LEGENDplex bead-base immunoassay.

(J) FITC-dextran fluorescence intensity.

(K) Protein concentration in the BALF.

Data are represented as means ± SEM (one-way ANOVA). ns, not significant, $*p < 0.05$; $**p < 0.01$; $***p < 0.001$.

See also Figure S6.

KEY RESOURCES TABLE

REAGENT or RESOURCE	SOURCE	IDENTIFIER
Antibodies		
FITC anti-mouse CD45 (Clone 30-F11)	BioLegend	Cat # 103108; RRID: AB_312973
APC/Cyanine7 anti-mouse CD45 (Clone 30-F11)	BioLegend	Cat # 103116; RRID: AB_312981
PE-Cy7 Hamster Anti-Mouse CD11c (Clone HL3)	BD Biosciences	Cat # 558079; RRID: AB_647251
Brilliant Violet 421 anti-mouse/human CD11b (Clone M1/70)	BioLegend	Cat # 101236; RRID: AB_11203704
PerCP/Cyanine5.5 anti-mouse/human CD11b	BioLegend	Cat # 101228; RRID: AB_893232
PE Rat Anti-Mouse Siglec-F (clone E50– 2440)	BD Bioscience	Cat # 552126; RRID: AB_394341
PerCP/Cyanine5.5 anti-mouse CD3 (clone 17A2)	BioLegend	Cat # 100218; RRID: AB_1595492
Brilliant Violet 510 anti-mouse CD19 (Clone 6D5)	BioLegend	Cat # 115546; RRID: AB_2562137
APC anti-mouse Ly-6G/Ly-6C (Gr-1) (Clone RB6–8C5)	BioLegend	Cat # 108412; RRID: AB_313377
APC/Cyanine7 anti-mouse Ly-6C (Clone HK1.4)	BioLegend	Cat # 128026; RRID: AB_10640120
PE anti-mouse CD64 (FcgRI) (Clone X54–5/7.1)	BioLegend	Cat # 139304; RRID: AB_10612740
Brilliant Violet 510 anti-mouse I-A/I-E (MHC-II) (Clone M5/114.15.2)	BioLegend	Cat # 107636; RRID: AB_2734168
FITC anti-mouse CD206 (MMR) (<C068C2)	BioLegend	Cat # 141704; RRID: AB_10901166
APC anti-mouse CD163 (Clone S15049I)	BioLegend	Cat # 155306; RRID: AB_2814060
PerCP/Cyanine5.5 anti-mouse CD36 (Clone HM36)	BioLegend	Cat # 102620; RRID: AB_2750188
Brilliant Violet 421 anti-mouse CD86 (Clone GL-1)	BioLegend	Cat # 105032; RRID: AB_2650895
InVivoMAb anti-mouse CD16/CD32	BioXCell	Cat # BE0307; RRID: AB_2736987
LC3B Rabbit Antibody	Cell Signaling Technology	Cat #B2775S; RRID:AB_915950
SQSTM1/p62 Rabbit Antibody	Cell Signaling Technology	Cat #B5114S; RRID:AB_10624872
beta Actin Antibody (C4)	Santa Cruz Biotechnology	Cat # 47778; RRID:AB_626632
Goat anti-Rabbit IgG (H + L) Secondary Antibody, HRP	Invitrogen	Cat # 31460; RRID: AB_228341
Goat anti-Mouse IgG (H + L) Secondary Antibody, HRP	Invitrogen	Cat # 31430; RRID: AB_228307
Chemicals, peptides, and recombinant proteins		
Collagenase Type 4	Worthington-Biochemicals	Cat # LS004186
High molecular weight polyinosine-polycytidylic acid (Poly(I:C))	InvivoGen	Cat #tlrl-pic-5; CAS # 31852-29-6
RBC Lysis Buffer (10X)	BioLegend	Cat #420302
Fluorescein isothiocyanate-dextran (FITC-Dextran)	Sigma Aldrich	Cat #46944-500mg-F; CAS # 60842-46-8
RPMI	Corning	Cat #10-040-CV
Fetal Bovine Serum	Omega Scientific	Cat # FB-01
Penicillin-Streptomycin Solution 100X	Omega Scientific	Cat # PS-20
Rapamycin	Thermo Fisher	Cat # PHZ1235
RIPA Lysis Buffer 10X	EMD Millipore	Cat # 20-188
PierceTM Protease and Phosphatase Inhibitor Mini Tablets, EDTA-free	Thermo Scientific	Cat# A32961
6x Laemmli SDS Sample Buffer	Bioland Scientific	Cat # SAB03-01
TAT peptide	Genscript	N/A

REAGENT or RESOURCE	SOURCE	IDENTIFIER
Critical commercial assays		
LEGENDplex™ Mouse Anti-Virus Response Panel (13-plex) with V-bottom Plate	BioLegend	Cat #740622
RNeasy Mini kit	Qiagen	Cat #74104
Pierce™ BCA Protein Assay Kit	ThermoFisher	Cat #23225
Deposited data		
Bulk RNA-seq data	This paper	GEO Accession: GSE227213
Experimental models: Cell lines		
THP1-Difluo™ hLC3 Cells	InvivoGen	Cat# thpdf-hlc3
Experimental models: Organisms/strains		
Mouse: C57Bl/6	Jackson Laboratory	Strain #:000664; RRID: IMSR_JAX:000664
Mouse: Atg5$^{fl/fl}$	Dr Noboru Mizushima (Tokyo Medicaland Dental University, Tokyo, Japan)	N/A
Mouse: Atg5^{KO}: Atg5$^{fl/fl}$-CD11c-Cre	Dr. Omid Akbari (University of Southern California, Los Angeles, CA)	N/A
Mouse: Tfeb$^{fl/fl}$	Dr. Babak Razani (University of Pittsburgh School of Medicine, Pittsburgh, PA)	N/A
Mouse: Tfeb^{TG}: Tfeb$^{fl/fl}$-CD11c-Cre	Dr. Omid Akbari (University of Southern California, Los Angeles, CA)	N/A
Mouse: GFP-LC3	Dr Noboru Mizushima (Tokyo Medicaland Dental University, Tokyo, Japan)	N/A
Software and algorithms		
FlowJo analysis software version 10	TreeStar	N/A
GraphPad Prism 7 Software	GraphPad	N/A
Partek Flow, version 10.0	Partek Inc	N/A
ImageJ	NIH	N/A
BZ-X Viewer 01.03.01.01	Keyence	N/A
NIS Elements AR 5.41.02	Nikon	N/A
Other		
CountBright absolute counting beads	Thermofisher	Cat #C36950